Nuclear Instruments and Methods in Physics Research B 512 (2022) 54–59

Contents lists available at ScienceDirect

Nuclear Inst. and Methods in Physics Research, B

journal homepage: www.elsevier.com/locate/nimb

Extending defect models for Si processing: The role of energy barriers for defect transformation, entropy and coalescence mechanism

Iván Santos [a,*], Ana Caballo [b], María Aboy [a], Luis A. Marqués [a], Pedro López [a], Lourdes Pelaz [a]

[a] Dpto. de Electricidad y Electrónica, E.T.S.I. de Telecomunicación, Universidad de Valladolid, Paseo Belén 15, 47011 Valladolid, Spain
[b] Institute for Molecules and Materials, Radboud University, Heyendaalseweg 135, 6525 AJ Nijmegen, The Netherlands

ARTICLE INFO

Keywords:
Silicon processing
Si self-interstitial clusters
Defect growth models
Atomistic simulations
Coalescence
Ostwald ripening

ABSTRACT

Emergent alternative Si processes and devices have promoted applications outside the usual processing temperature window and the failure of traditional defect kinetics models. These models are based on Ostwald ripening mechanisms, assume pre-established defect configurations and neglect entropic contributions. We performed molecular dynamics simulations of self-interstitial clustering in Si with no assumptions on preferential defect configurations. Relevant identified defects were characterized by their formation enthalpy and vibrational entropy calculated from their local vibrational modes. Our calculations show that entropic terms are key to understand defect kinetics at high temperature. We also show that for each cluster size, defect configurations may appear in different crystallographic orientations and transformations among these configurations are often hampered by energy barriers. This induces the presence of non-expected small-size defect cluster configurations that could be associated to optical signals in low temperature processes. At high temperatures, defect dynamics entails mobility and ripening through a coalescence mechanism.

1. Introduction

Ion implantation is a widely used technology to introduce dopants in semiconductor devices. As energetic dopants penetrate into the substrate, atomic displacements occur and the lattice is damaged producing Frenkel pairs. After implantation, thermal annealing treatments are performed to increase the concentration of dopants in substitutional positions and to recover the damage generated during the implantation step. As active dopants occupy lattice positions, a Si self-interstitial excess is generated [1]. These particles diffuse and interact during annealing treatments, resulting in the formation of more complex self-interstitial clusters. Their evolution is conventionally modeled through an Ostwald Ripening mechanism, in which big and more stable defects grow by the capture of Si self-interstitials emitted by smaller and less stable defects. The ripening process is slow because only one self-interstitial is exchanged at a time, and cluster energetics determine its evolution.

Small clusters are not visible through experiments but there are experimental signals that reveal their presence [2]. Their structure and energy are inferred through theoretical calculations, but generally only the most stable configuration for each cluster size is considered in the models [2–5]. For larger cluster sizes, {113} rod-like defects and {111} dislocation loops are observed experimentally through Transmission Electron Microscopy. The combination of defect growth models and experimental observations have provided a good description of defect structures generated for a given combination of implantation dose and thermal annealing temperature [6]. Thus, {113} defects are observed after 10^{12}–10^{14} cm^{-2} implant doses and annealing treatments up to 700–800 °C, while {111} dislocation loops are the predominant defect observed for implant doses above 10^{14} cm^{-2} and annealing treatments above 800 °C.

Nevertheless, there are a few experimental results that cannot be explained from this unified picture. On the one hand, extended {001} loops have been obtained after few nanoseconds in sub-melting laser annealed ion-implanted Si [7]. The formation of these extended defects is incompatible with an Ostwald Ripening growth process as it would require more than a few nanoseconds for these extended defects to form through the dissolution of small clusters and the growth of the larger and more stable clusters. In addition, {001} loops have a higher formation energy than {111} loops, so its formation is not energetically favorable.

On the other hand, the intense W photoluminescence (PL) line that appears on as-irradiated Si is associated to Si tri-interstitial (I_3) clusters [8–11]. Nevertheless, none of the defect structures of the I_3 cluster proposed as candidates for W-PL centers corresponds to the most stable I_3 configuration [5,10,11]. Consequently, the formation of W

* Corresponding author.
E-mail address: ivasan@tel.uva.es (I. Santos).

https://doi.org/10.1016/j.nimb.2021.12.002
Received 27 September 2021; Received in revised form 29 November 2021; Accepted 1 December 2021

PL centers in irradiated Si would be extremely unlikely according to conventional models of defect kinetics.

It is therefore necessary to extend actual defect models in the low and in the high temperature regimes. In this work we discuss how the variability of defect configurations affects in low temperature processes, and how alternative defect growth mechanisms have to be considered in the high temperature regime. For this purpose, we have combined our previous findings on atomistic modeling of Si self-interstitial clusters with new results that help to extend traditional models of defect kinetics.

2. Variability of defect configurations

Defect clusters of a given size may appear in different configurations. There are several relatively complex techniques for exploring the configurational landscape of defects, such as hyperdynamics, parallel replica dynamics, or temperature-accelerated dynamics for example [12]. These techniques are very useful for systems where infrequent thermally activated events govern the atom dynamics, and they allow accessing long-time dynamics simulations. Another approach consists on long time Molecular Dynamics (MD) simulations at elevated temperature where a large number of defect configurations are visited. This sampling method can also provide information on their thermodynamic free energy [13–15] and it is the method used in the present study.

We have used LAMMPS code [16] to perform MD simulations for exploring the configurational landscape of small Si self-interstitial defect clusters ($I_{n\leq 10}$) from atom dynamics during annealing simulations. We have used the Tersoff empirical potential within its third parametrization to describe the Si–Si interactions [17]. This empirical potential has been shown to properly describe the structure of point [18] and extended defects [19,20] in crystalline Si (*c*-Si). Simulations have been performed at 1200 K (which corresponds to half of the melting temperature for this empirical potential) during 25 ns, and the simulation time step was 0.5 fs. The simulation cell was cubic, it had a lateral dimension of $6a_0$ (being a_0 the lattice parameter of *c*-Si), and it contained $1728+n$ atoms (with $n = 2, 3 \dots 10$ the excess of Si interstitials). Extra atoms were placed close enough so they easily form a defect cluster as the simulation starts, but no particular initial configuration was forced. Periodic boundary conditions have been applied in all spatial directions. Atomic positions were averaged every 1000 steps during simulations to filter out thermal vibrations, and resulting averaged configurations were relaxed using a conjugated-gradient algorithm.

For each cluster size, we have represented the formation energies of defect configurations obtained after conjugated-gradient relaxations along the simulation time, which were calculated as

$$E_f(I_n) = E_T(I_n) - \frac{N_{cSi}+n}{N_{cSi}} E_T(cSi) \quad (1)$$

being $E_T(I_n)$ the total energy at 0 K of the simulation cell containing the I_n defect, which is embedded in crystalline simulation cell of N_{cSi} Si atoms with a total energy equal to $E_T(cSi)$. We have identified the defect configurations corresponding to the different formation energy levels observed.

As an example, we have shown in Fig. 1 the results obtained for the I_3 defect. The energy level associated to the most stable I_3 atomic configuration is a chain-like defect oriented along the ⟨011⟩ direction with $E_f = 7.95$ or 2.65 eV per interstitial atom. This minimum-energy configuration found with the Tersoff empirical potential slightly differs from the minimum-energy configuration obtained with *ab initio* calculations [5,21,22]. The *ab initio* minimum-energy structure has been also observed in our simulations with a slightly higher formation energy of 8.29 eV or 2.76 eV per interstitial atom. Both structures correspond to ⟨011⟩ chain-like defects. We have also obtained other chain-like defects configurations oriented along the ⟨011⟩ direction. Our simulations revealed frequent transitions between this family of ⟨011⟩ chain-like defects, which have been indicated by the red oval in Fig. 1 and labeled as "⟨011⟩ chain-like variations". We have also identified another family of defects consisting of compact Si tri-interstitial clusters in the {001} plane. A representative example of these defects has been shown in the inset of Fig. 1, whose structure is very similar to the well-known Arai tetra-interstitial cluster [23] (I_4^{Arai}) but with only three Si self-interstitial atoms rather than four. Interestingly, one of the defect candidates for W PL-center appeared from these simulations ($I_3 - V$ defect in Refs. [10,11], not shown in Fig. 1), but its formation energy is 8.69 eV or 2.90 eV per interstitial atom, higher than the most stable defect found in Fig. 1.

Analogous annealing simulations for other cluster sizes have also revealed that the most frequent defect configurations mainly correspond to ⟨011⟩ chain-like and the {001} compact-like defect structures. Nevertheless, in the case of I_4, the compact I_4^{Arai} configuration strongly dominates due to its high stability [24], although some chain-like configuration have also been obtained. ⟨011⟩ chain-like Si self-interstitial clusters are the core structure of extended {113} rod-like defects [25,26], while {001} compact-like defects are agglomerates of the Arai tetra-interstitial [23] (I_4^{Arai}) and the building block of {001} loops [20]. In addition, both types of defect structures (⟨011⟩ chain-like and the {001} compact-like defects) have been observed in simulations of the initial stages of Si self-interstitial agglomeration in *c*-Si [13,27].

We have also found that transitions between configurations within the same defect family (i.e. among ⟨011⟩ chain-like defects or among {001} compact-like defects) are frequent, but it is not so frequent the transition between different defect families (i.e. from ⟨011⟩ chain-like defects to {001} compact-like defects or *vice versa*). This indicates that there are significant energy barriers that prevent these "inter-family" transitions. Using the activation-relaxation technique for exploring the energy landscape around defect structures, it has been recently shown that the energy barrier for exiting the I_4^{Arai} compact defect ranges from 1 to ∼3 eV [28]. Using this technique, energy barriers from ∼1 to ∼2.3 eV were found for the transition between chain-like and compact-like I_n defects, with $n = 2, 3, 4$ [29]. In low temperature processing, these energy barriers would prevent "inter-family" transitions and would eventually block clusters from reaching the minimum-energy configurations.

It is worth noting that, for some cluster sizes, our annealing simulations have revealed that the more frequent defect configuration does not correspond to the minimum-energy configuration at $T = 0$ K. This fact agrees with previous studies [14], and indicates that the sampling method used in the present work correctly takes into account the thermodynamics of the system and not only the potential energy landscape as other methods exclusively consider.

Due to the relevance of ⟨011⟩ chain-like and the {001} compact-like defects, we have investigated how these structures grow. For this purpose, we have added an extra Si interstitial atom to a given I_n of a particular family (⟨011⟩ chain-like or {001} compact-like) to find the I_{n+1} structure of the same family. We have performed MD annealing simulations at 1000 K of the $I_n + I$ system to favor atom dynamics. Defect structures visited during atom dynamics where relaxed using a conjugate gradient algorithm, and their formation energies at 0 K was evaluated as indicated by Eq. (1). For these calculations, we have used cubic simulation cells with lateral dimensions of $8a_0$ containing $8000+n$ atoms, being $n = 2, 3 \dots 16$ the excess of Si interstitials. We have represented the obtained formation energies in Fig. 2.a. It can be noted that formation energies of ⟨011⟩ chain-like defects decrease with size, while formation energies of {001} compact-like defects show local minima at the multiple-of-four configurations. These favored compact-like configurations are observed in MD simulations that follow the dynamics of a large number of self-interstitials at elevated temperatures [13,27], and are also consistent with the "magic numbers" obtained from inverse modeling [2]. Most compact-like defects observed in these MD simulations correspond to isolated I_4^{Arai} or other multiple of this structure ($I_8, I_{12}, I_{16} \dots$). Other intermediate sizes ($n = 5, 6, 7$) hardly

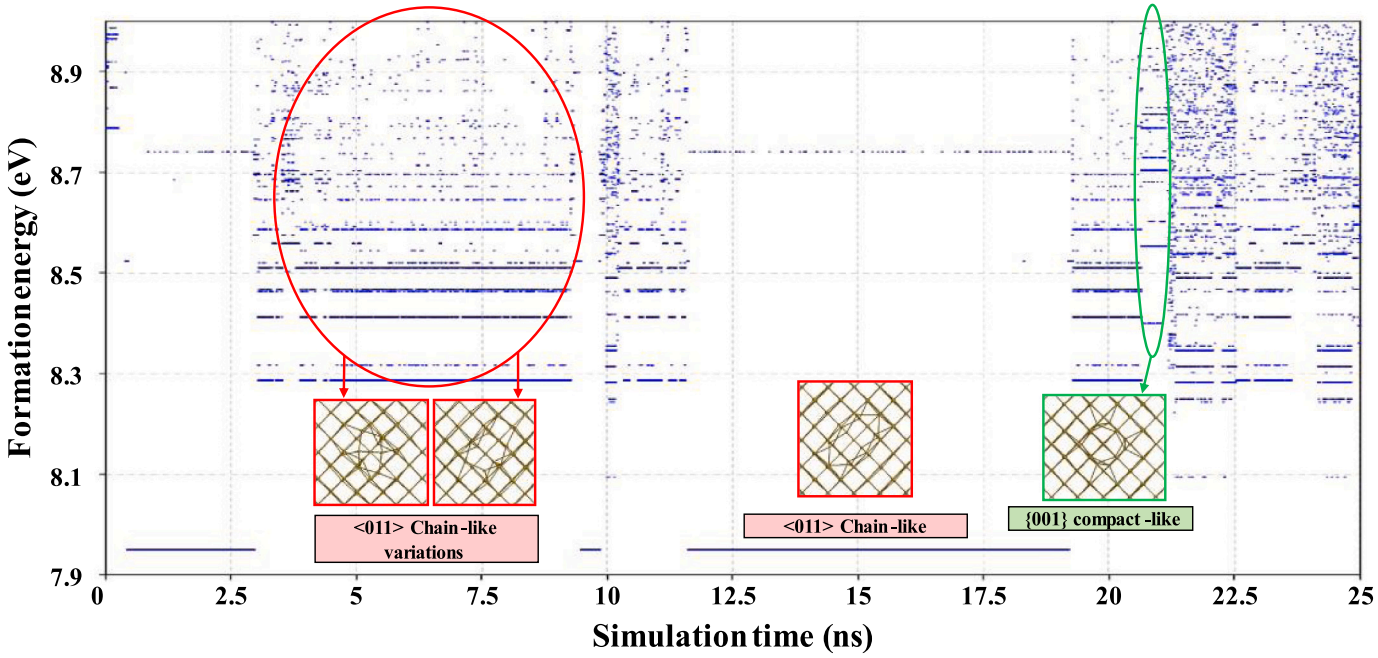

Fig. 1. Formation energy of different configurations of I_3 defect obtained during the annealing MD simulation at 1200 K. Ovals group energies of defects that correspond to slight variations of a core defect structure. Snapshots show representative atomic configurations projected along the ⟨001⟩ direction of defect structures found for the ⟨011⟩ chain-like and the {001} compact-like defect structures. Lines shown in snapshots represent atomic bonds.

appear, although it can be seen from Fig. 2.a that apparently there is not a significant energy difference to block its growth.

For a correct description of the evolution of defects, it is necessary to resort to the Gibbs free energy where there is also has an entropy contribution in addition to the formation energy of defects [30]:

$$G = U - TS + pV \tag{2}$$

In the case of defect clusters, their entropy is commonly dominated by their vibrational entropy [30,31], which can be evaluated from their local vibrational modes as [31]

$$S_{vib} = k_B \sum_{i=1}^{3N_{at}} \left[\frac{\beta h \nu_i}{2} \coth\left(\frac{\beta h \nu_i}{2}\right) - \ln\left(2\sinh\left(\frac{\beta h \nu_i}{2}\right)\right)\right] \tag{3}$$

being k_B the Boltzmann constant, $\beta = \frac{1}{k_B T}$, T the temperature in K, h the Planck's constant, ν_i the frequency of the ith local vibrational mode of the simulation cell with N_{at} atoms. Local vibrational modes were evaluated within the harmonic approximation through the calculation of the Dynamical Matrix of the system [32]. The defect vibrational entropy of formation is evaluated as [31]

$$\Delta S_{vib}(I_n) = S_{vib}(I_n) - S_{vib}(cSi) \tag{4}$$

Then, the defect Helmholtz free formation energy is calculated as

$$F_f(I_n) = E_f(I_n) - T\Delta S_{vib}(I_n) \tag{5}$$

which agrees with its Gibbs formation energy for the case of $p = 0$.

We have represented in Fig. 2.b the entropic contribution $T \cdot \Delta S_{vib}$ at 1200 K to the Helmholtz free energy. Higher values of this term contributes to make the defect more favorable (as it enters with a negative sign in Eq. (5)). It can be seen from Fig. 2.b that for the ⟨011⟩ chain-like defects there are slight local maxima (minima) at odd (even) cluster sizes. As the cluster size increases, the entropic contribution is reduced and even and odd sizes have closer values. In the case of {001} compact-like defects, local minima occur for $4m - 1$ sizes (being $m = 2, 3 \ldots$).

Helmholtz free formation energies at 1200 K are represented in Fig. 2.c. In the case of the ⟨011⟩ chain-like defects, the curve becomes slightly more stepped with respect to the one shown in Fig. 2.a, with odd cluster sizes being less energetic due to the entropic-stabilization effect. In the case of the {001} compact-like defects, local energy minima occur for $4m$ sizes (being $m = 1, 2, 3 \ldots$) being the energy per atom for intermediate sizes (specially for I_5, I_6 and I_7) significantly higher. This implies that I_5, I_6 and I_7 emit Si self-interstitials more easily than the I_4^{Arai} cluster. This makes it difficult their growth through an Ostwald Ripening process towards larger sizes because Si self-interstitials trapped by larger clusters will be released before other Si self-interstitials are made available by smaller defects. Consequently, in a pure "one-by-one Si self-interstitial interchange mechanism", it is difficult to form clusters larger than the I_4^{Arai} cluster. This explains the large concentration of isolated compact tetra-interstitials observed in the simulations [13,27].

3. Ostwald ripening and coalescence growth mechanisms

Models based on the Ostwald Ripening mechanism have been successfully used to explain defect growth in most Si processing conditions of ion implantation and annealing. However, the formation of {001} loops during Si laser processing highlights the need for considering alternative defect growth mechanisms. For a better understanding of defect growth mechanisms at high temperatures, we have performed a MD annealing simulation at 1900 K (which correspond to 80% of the melting temperature for Tersoff empirical potential) analogous to those described in Section 2. In this case, we have used a cubic simulation cell with lateral dimension of $8a_0$, where we have embedded two isolated Si self-interstitial compact-like clusters laying in the same (001) plane: a I_4^{Arai} defect and compact penta-interstitial ($I_5 \equiv I_4^{Arai} + I$) separated by $3\sqrt{2}a_0$. This initial configuration can be seen in Fig. 3, where for clarity only atoms distant more than 0.7 Å from lattice positions are represented.

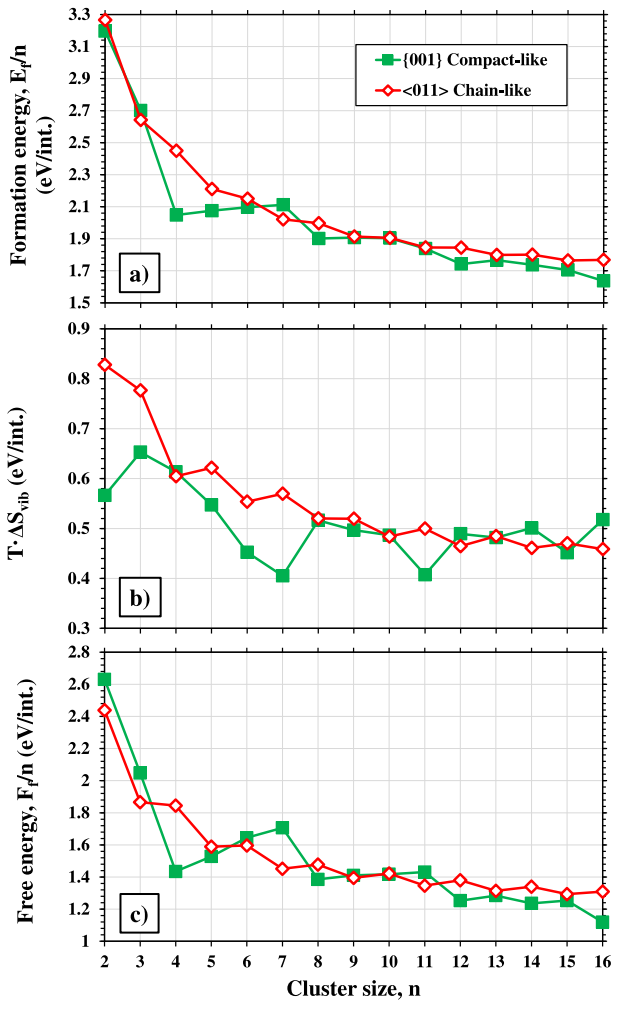

Fig. 2. (a) Formation energy, (b) Entropic contribution ($T \cdot \Delta S_{vib}$) at 1200 K and (c) Helmholtz free formation energy per interstitial atom for ⟨011⟩ chain-like and the {001} compact-like defects.

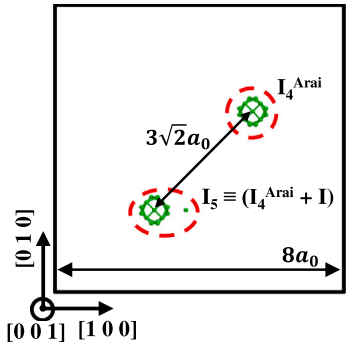

Fig. 3. Schematic snapshot of the initial configuration consisting on a I_4^{Arai} defect and compact penta-interstitial ($I_4^{Arai} + I$) projected along the (001) direction (see text for details). For clarity, we have only represented atoms distant more than 0.7 Å from a lattice position in the snapshots of defect structures.

According to an Ostwald Ripening process, the penta-interstitial would emit a Si self-interstitial atom, which would be free to move, transforming into a I_4^{Arai} defect. Due to the reduced size of the simulation cell and to the stability of the I_4^{Arai} defect, the released Si self-interstitial would interact with one of the two I_4^{Arai} defects present in the simulation cell much before one of these defects release another Si self-interstitial. Thus, both I_4^{Arai} defects are expected to continuously interchange a self-Si interstitial atom. The result of MD annealing simulation at 1900 K follows this behavior up to some point, but there are substantial differences that cannot be explained according to a pure Ostwald Ripening process.

We have represented in Fig. 4.a the root mean square displacement (RMSD) of the system during the simulation, which is calculated as

$$RMSD(t) = \sqrt{\frac{\sum_{i=1}^{N_{at}} \left(\vec{r}_i(t) - \vec{r}_i(0)\right)^2}{N_{at}}} \quad (6)$$

where $\vec{r}_i(t)$ is the vector position of atom i at time t. The RMSD presents several pseudo-plateaus with a small slope followed by rapid increments, which have been indicated with odd and even numbers respectively in Fig. 4.a. During the initial plateau (label (1) in Fig. 4.a) the I atom of the I_5 cluster starts moving around the I_4^{Arai} core in the (001) plane. This movement destabilizes the structure of the defect, which at some point becomes amorphous-like, as it is shown for a particular example in Fig. 4.b. This defect changes continuously its structure, and each structural change is accompanied by a slight random displacement of its center of mass. This results in a small increase in the RMSD, as it can be seen in Fig. 4.a.(1). During this random movement of the amorphous I_5 defect, the other I_4^{Arai} defect remains unaltered.

At some point the amorphous I_5 defect releases a Si self-interstitial, which freely moves in the simulation cell and results in the rapid increase of the RMSD shown in Fig. 4.a.(2). During this stage, both I_4 defects adopt the compact-like structure, as it is shown in Fig. 4.c. In addition to the two I_4^{Arai} structures, Fig. 4.c shows the free Si self-interstitial in the so called extended configuration [18].

The free Si self-interstitial eventually interacts with one of the I_4^{Arai} defects (Fig. 4.a.(3)), whose structure is destabilized and starts slowly moving due to the continuous changes of its structure (and the increment in the RMSD is reduced but not suppressed). During this random movement, the resulting amorphous I_5 defect eventually reaches the other I_4^{Arai} defect, and both defects merge together in an amorphous I_9 defect, as shown in 4.d. Therefore, the formation of a larger cluster has not been accomplished through an Ostwald Ripening process, but through the coalescence of two defects. Although this process might be somehow forced due to the reduced dimensions of the simulation cell used, it has also been observed in much larger simulations cells with Si self-interstitial atoms at a temperature close to the melting point of *c*-Si [20,27,33].

Once the I_9 defect has been formed, there are different possibilities for its evolution. It can release a Si self-interstitial atom (Fig. 4.a.(4, 6, 8)), as it has been represented in Fig. 4.e for a representative case. The structure of the resulting amorphous I_8 defect continuously change, and it might internally reorder part of its structure similarly to two I_4^{Arai} defects, as represented in Fig. 4.f.

The structure of the I_9 defect may also change (during Fig. 4.a.(5, 7)) resulting in: (i) amorphous structures (Fig. 4.g); (ii) the nucleation of I_4^{Arai}-like structures (Fig. 4.h); or even (iii) the transition to a different defect family, as shown in Fig. 4.i where a chain-like defect structure is visited. Therefore, the configuration variability of amorphous diffusive defects present at high temperatures does not only result in the formation of larger defects through a coalescence mechanism, but it also facilitates the transition among different defect families for large defect sizes that eventually would result in the nucleation of extended defects in *c*-Si.

4. Conclusions

In this work we have discussed how traditional models used to describe defect growth in *c*-Si should be extended to capture relevant features in actual Si processing conditions. In the case of low temperature processes, it is necessary to consider additional configurations to the most stable ones. These additional configurations, in

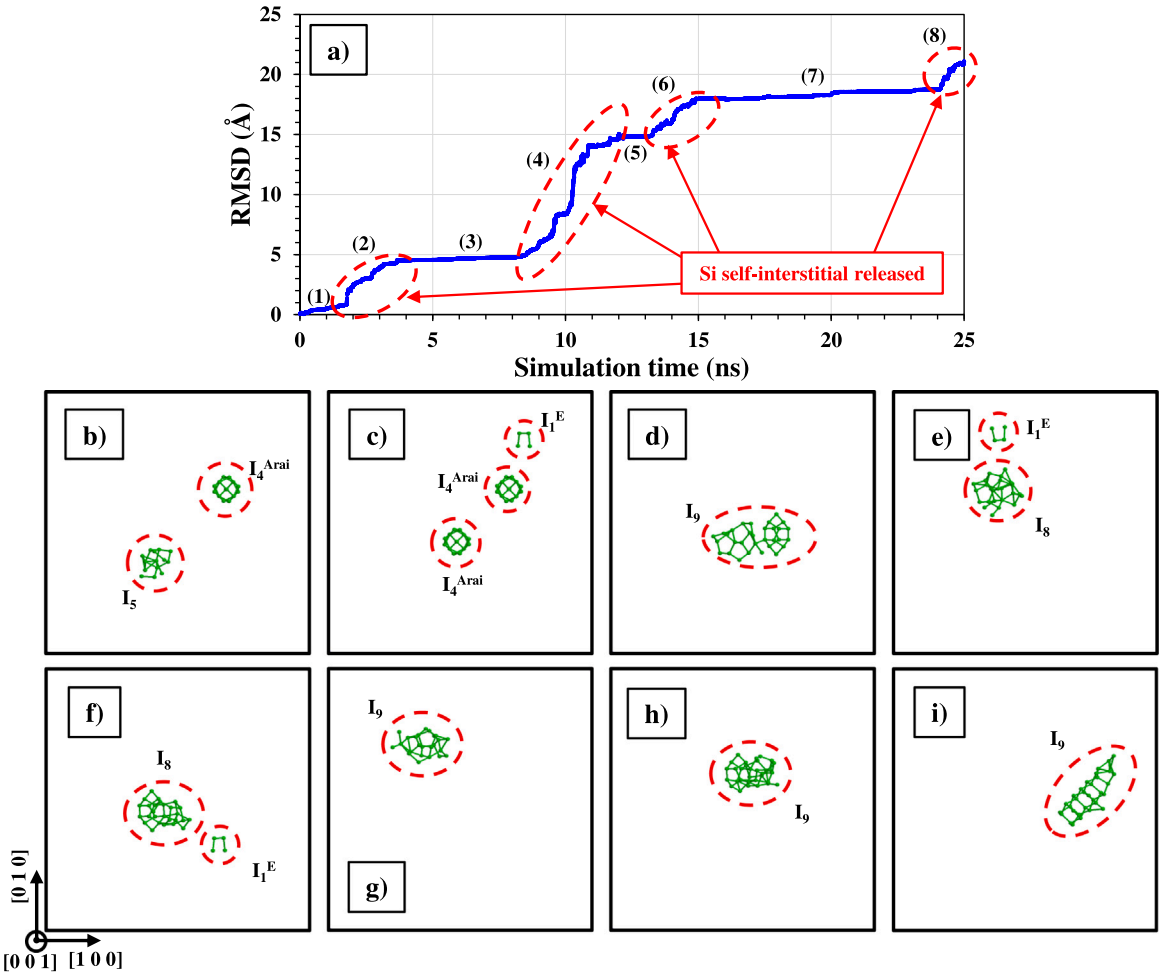

Fig. 4. Summary of results for the annealing MD simulation at 1900 K: (a) root mean square displacement (RMSD) during simulation; (b–i) snapshots of different defect structures obtained from the simulation projected along the (001) direction (see text for details). For clarity, we have only represented atoms distant more than 0.7 Å from a lattice position in the snapshots of defect structures.

combination with transition energy barriers, explain the presence of non-minimum-energy defect structures in low temperature processing conditions. For high temperature processing, it is important to consider (i) defect entropy and (ii) defect diffusion as the result of the transition among different configurations. The Ostwald ripening growth mechanism should be complemented with the coalescence mechanism in which mobile defects merge together to form larger defects.

CRediT authorship contribution statement

Iván Santos: Conception and design of study, Investigation, Software, Acquisition of data, Analysis and interpretation of data, Visualization, Writing – original draft, Writing – review & editing. **Ana Caballo:** Conception and design of study, Investigation, Software, Acquisition of data, Analysis and interpretation of data, Writing – original draft, Writing – review & editing. **María Aboy:** Conception and design of study, Investigation, Software, Acquisition of data, Analysis and interpretation of data, Writing – original draft, Writing – review & editing. **Luis A. Marqués:** Conception and design of study, Investigation, Software, Acquisition of data, Analysis and interpretation of data, Writing – original draft, Writing – review & editing. **Pedro López:** Conception and design of study, Investigation, Analysis and interpretation of data, Writing – original draft, Writing – review & editing, Funding acquisition. **Lourdes Pelaz:** Conception and design of study, Investigation, Analysis and interpretation of data, Writing – original draft, Writing – review & editing, Funding acquisition, Supervision.

Declaration of competing interest

The authors declare that they have no known competing financial interests or personal relationships that could have appeared to influence the work reported in this paper.

Acknowledgment

This work has been supported by the spanish Ministerio de Ciencia e Innovación under Project No. PID2020-115118GB-I00.

All authors approved the version of the manuscript to be published.

References

[1] L. Pelaz, G.H. Gilmer, M. Jaraiz, S.B. Herner, H.-J. Gossmann, D.J. Eaglesham, G. Hobler, C.S. Rafferty, J. Barbolla, Modeling of the ion mass effect on transient enhanced diffusion: Deviation from the "+1" model, Appl. Phys. Lett. 73 (10) (1998) 1421–1423, http://dx.doi.org/10.1063/1.121963.

[2] N.E.B. Cowern, G. Mannino, P.A. Stolk, F. Roozeboom, H.G.A. Huizing, J.G.M. van Berkum, F. Cristiano, A. Claverie, M. Jaraíz, Energetics of self-interstitial clusters in Si, Phys. Rev. Lett. 82 (1999) 4460–4463, http://dx.doi.org/10.1103/PhysRevLett.82.4460.

[3] A. Bongiorno, L. Colombo, F. Cargnoni, C. Gatti, M. Rosati, Evolution of energetics and bonding of compact self-interstitial clusters in Si, Europhys. Lett. 50 (2000) 608–614, http://dx.doi.org/10.1209/epl/i2000-00313-4.

[4] M.P. Chichkine, M.M. De Souza, E.M. Sankara Narayanan, Growth of precursors in silicon using pseudopotential calculations, Phys. Rev. Lett. 88 (2002) 085501, http://dx.doi.org/10.1103/PhysRevLett.88.085501.

[5] S. Lee, G.S. Hwang, Growth and shape transition of small silicon self-interstitial clusters, Phys. Rev. B 78 (2008) 045204, http://dx.doi.org/10.1103/PhysRevB.78.045204.
[6] F. Cristiano, N. Cherkashin, X. Hebras, P. Calvo, Y. Lamrani, E. Scheid, B. de Mauduit, B. Colombeau, W. Lerch, S. Paul, A. Claverie, Ion beam induced defects in crystalline silicon, Nucl. Instrum. Methods Phys. Res. B 216 (2004) 46—56, http://dx.doi.org/10.1016/j.nimb.2003.11.019.
[7] Y. Qiu, F. Cristiano, K. Huet, F. Mazzamuto, G. Fisicaro, A. La Magna, M. Quillec, N. Cherkashin, H. Wang, S. Duguay, D. Blavette, Extended defects formation in nanosecond laser-annealed ion implanted silicon, Nano Lett. 14 (2014) 1769–1775, http://dx.doi.org/10.1021/nl4042438.
[8] G. Davies, E.C. Lightowlers, Z.E. Ciechanowska, The 1018 mev (W or I1) vibronic band in silicon, J. Phys. C: Solid State Phys. 20 (1987) 191–205, http://dx.doi.org/10.1088/0022-3719/20/2/003.
[9] G. Davies, The optical properties of luminescence centres in silicon, Phys. Rep. 176 (1989) 83–188, http://dx.doi.org/10.1016/0370-1573(89)90064-1.
[10] A. Carvalho, R. Jones, J. Coutinho, P.R. Briddon, Density-functional study of small interstitial clusters in Si: Comparison with experiments, Phys. Rev. B 72 (2005) 155208, http://dx.doi.org/10.1103/PhysRevB.72.155208.
[11] I. Santos, M. Aboy, P. López, L.A. Marqués, L. Pelaz, Insights on the atomistic origin of X and W photoluminescence lines in c-Si from ab initio simulations, J. Phys. D: Appl. Phys. 49 (2016) 075109, http://dx.doi.org/10.1088/0022-3727/49/7/075109.
[12] R.J. Zamora, D. Perez, E. Martinez, B.P. Uberuaga, A.F. Voter, Accelerated molecular dynamics methods in a massively parallel world, in: W. Andreoni, S. Yip (Eds.), Handbook of Materials Modeling : Methods: Theory and Modeling, Springer International Publishing, 2019, pp. 1–28, http://dx.doi.org/10.1007/978-3-319-42913-7_25-2.
[13] S.S. Kapur, T. Sinno, Detailed microscopic analysis of self-interstitial aggregation in silicon. I. Direct molecular dynamics simulations of aggregation, Phys. Rev. B 82 (2010) 045205, http://dx.doi.org/10.1103/PhysRevB.82.045205.
[14] S.S. Kapur, A.M. Nieves, T. Sinno, Detailed microscopic analysis of self-interstitial aggregation in silicon. II. Thermodynamic analysis of single clusters, Phys. Rev. B 82 (2010) 045206, http://dx.doi.org/10.1103/PhysRevB.82.045206.
[15] C.Y. Chuang, A. Sattler, T. Sinno, Thermodynamic and morphological analysis of large silicon self-interstitial clusters using atomistic simulations, J. Appl. Phys. 117 (2015) 135706, http://dx.doi.org/10.1063/1.4917049.
[16] S. Plimpton, Fast parallel algorithms for short-range molecular dynamics, J. Comput. Phys. 117 (1995) 1–19, http://dx.doi.org/10.1006/jcph.1995.1039, URL https://www.lammps.org/.
[17] J. Tersoff, Empirical interatomic potential for silicon with improved elastic properties, Phys. Rev. B 38 (1988) 9902–9905, http://dx.doi.org/10.1103/PhysRevB.38.9902.
[18] L.A. Marqués, L. Pelaz, P. Castrillo, J. Barbolla, Molecular dynamics study of the configurational and energetic properties of the silicon self-interstitial, Phys. Rev. B 71 (2005) 085204, http://dx.doi.org/10.1103/PhysRevB.71.085204.
[19] L.A. Marqués, M. Aboy, K.J. Dudeck, G.A. Botton, A.P. Knights, R.M. Gwilliam, Modeling and experimental characterization of stepped and v-shaped 311 defects in silicon, J. Appl. Phys. 115, 143514. http://dx.doi.org/10.1063/1.4871538.
[20] L.A. Marqués, M. Aboy, M. Ruiz, I. Santos, P. López, L. Pelaz, 001 loops in silicon unraveled, Acta Mater. 166 (2019) 192–201, http://dx.doi.org/10.1016/j.actamat.2018.12.052.
[21] D.A. Richie, J. Kim, S.A. Barr, K.R.A. Hazzard, R. Hennig, J.W. Wilkins, Complexity of small silicon self-interstitial defects, Phys. Rev. Lett. 92 (2004) 045501, http://dx.doi.org/10.1103/PhysRevLett.92.045501.
[22] Y.A. Du, R.G. Hennig, T.J. Lenosky, J.W. Wilkins, From compact point defects to extended structures in silicon, Eur. Phys. J. B 57 (2007) 229–234, http://dx.doi.org/10.1140/epjb/e2007-00176-5.
[23] N. Arai, S. Takeda, M. Kohyama, Self-interstitial clustering in crystalline silicon, Phys. Rev. Lett. 78 (1997) 4265–4268, http://dx.doi.org/10.1103/PhysRevLett.78.4265.
[24] S.S. Kapur, T. Sinno, Entropic origins of stability in silicon interstitial clusters, Appl. Phys. Lett. 93 (2008) 221911, http://dx.doi.org/10.1063/1.3042096.
[25] J. Kim, F. Kirchhoff, J.W. Wilkins, F.S. Khan, Stability of Si-interstitial defects: From point to extended defects, Phys. Rev. Lett. 84 (2000) 503–506, http://dx.doi.org/10.1103/PhysRevLett.84.503.
[26] L.A. Marqués, L. Pelaz, I. Santos, P. López, M. Aboy, Structural transformations from point to extended defects in silicon: A molecular dynamics study, Phys. Rev. B 78 (2008) 193201, http://dx.doi.org/10.1103/PhysRevB.78.193201.
[27] L.A. Marqués, M. Aboy, M. Ruiz, I. Santos, P. López, L. Pelaz, Molecular dynamics simulation of the early stages of self-interstitial clustering in silicon, Mater. Sci. Semicond. Process. 42 (2016) 235–238, http://dx.doi.org/10.1016/j.mssp.2015.07.020.
[28] A. Jay, C. Huet, N. Salles, M. Gunde, L. Martin-Samos, N. Richard, G. Landa, V. Goiffon, S. De Gironcoli, A. Hémeryck, N. Mousseau, Finding reaction pathways and transition states: r-ARTn and d-ARTn as an efficient and versatile alternative to string approaches, J. Chem. Theory Comput. 16 (2020) 6726–6734, http://dx.doi.org/10.1021/acs.jctc.0c00541.
[29] D. Calvo, Characterization And Dynamics of Si Self-Interstitial Clusters by Self-Learning Kinetic Monte Carlo Simulations (Master Thesis), University of Valladolid, 2016, URL http://uvadoc.uva.es/handle/10324/20512.
[30] C. Freysoldt, B. Grabowski, T. Hickel, J. Neugebauer, G. Kresse, A. Janotti, C.G. Van de Walle, First-principles calculations for point defects in solids, Rev. Modern Phys. 86 (2014) 253–305, http://dx.doi.org/10.1103/RevModPhys.86.253.
[31] A. Walsh, A.A. Sokol, C.R.A. Catlow, Free energy of defect formation: Thermodynamics of anion Frenkel pairs in indium oxide, Phys. Rev. B 83 (2011) 224105, http://dx.doi.org/10.1103/PhysRevB.83.224105.
[32] M.T. Dove, Structure and Dynamics: An Atomic View of Materials, Oxford University Press, 2003.
[33] L.A. Marqués, M. Aboy, I. Santos, P. López, F. Cristiano, A. La Magna, K. Huet, T. Tabata, L. Pelaz, Ultrafast generation of unconventional 001 loops in Si, Phys. Rev. Lett. 119 (2017) 205503, http://dx.doi.org/10.1103/PhysRevLett.119.205503.